ELSEVIER

International Journal of Heat and Fluid Flow 23 (2002) 844–854

International Journal of HEAT AND FLUID FLOW

www.elsevier.com/locate/ijhff

Viscous effects in liquid encapsulated liquid bridges

Duane T. Johnson *

Department of Chemical Engineering, University of Alabama, A 127 Bevil Building, P.O. Box 870203, Tuscaloosa, AL 35487-0203, USA

Received 10 January 2001; accepted 13 March 2002

Abstract

An analytical derivation of the surface deflections and the streamfunctions for the flow inside a liquid encapsulated liquid bridge has been derived using an asymptotic expansion about a small capillary number. The model assumes an initially flat and cylindrical interface under the assumption that the densities of both fluids are equal. To simplify the analysis, the top and bottom walls are assumed to be stress-free and the Reynolds number is assumed to be negligible. Flow is generated either by a moving outer wall (shear-driven flow) or by applying a temperature difference across the top and bottom walls (Marangoni-driven flow). The resulting equations show that for the shear-driven flow, as the viscosity ratio increases, the surface deflections increase monotonically. For the Marangoni-driven flow there exist values of the viscosity ratio where the surface deflections reach a minimum and then switch signs. This investigation shows that it may be possible in more realistic systems to use an outer encapsulating liquid of the proper viscosity ratio to stabilize the liquid–liquid interface during float zone crystal growth.

Keywords: Thermocapillarity; Marangoni flow; Liquid bridges; Shear-driven flow

1. Introduction

The liquid bridge has received much attention in the last two decades as a model system to describe the float zone technique (Hurle, 1994; Rybicki and Floryan, 1983a,b; Wanschura et al., 1995). The float zone is used in the production of high purity silicon where an amorphous rod of silicon is passed through a ring heater. The ring heater melts the rod and creates a suspended "bridge" of liquid between the amorphous rod and the solidified crystal. If the height of the liquid bridge becomes too large, the liquid bridge will break and interrupt the solidification. It is therefore of practical importance to understand the stability of the liquid bridge during the float zone process.

There is interest in applying the float zone technique to the production of compound semiconductors, such as gallium arsenide (GaAs). However, when GaAs is melted it decomposes into its constituents of gallium and arsenic gas. In a Bridgman configuration, this decomposition is avoided by placing a liquid encapsulant of boron oxide (B_2O_3) around the GaAs, which lowers its vapor pressure. The question is can we place a liquid encapsulant around a liquid bridge? If so, how does the fluid behavior of the liquid encapsulant affect the stability of the liquid bridge?

If we observe the liquid encapsulated float zone process, we notice that there are two phenomena that drive fluid motion: buoyancy-driven convection and surface tension-driven convection. The temperature gradients generated by the ring heater cause both buoyancy-driven convection in the inner and outer fluids, as well as a surface tension-driven convection (Marangoni convection) at the liquid–liquid interface.

One interesting question that we may ask about the liquid encapsulated liquid bridge is what role does the viscosity play in the stability of the liquid–liquid interface? On one hand, as the viscosity is increased, the thicker fluid would act as a rigid plate and help stabilize the interface. On the other hand, as the viscosity is increased, the normal and tangential stresses on the interface are increased, therefore destabilizing the interface.

To answer this question, the stability of the interface in an idealized liquid encapsulated liquid bridge configuration will be studied. The fluid motion will be

* Tel.: +205-348-6450; fax: +205-348-7558.
E-mail address: djohnson@coe.eng.ua.edu (D.T. Johnson).

0142-727X/02/$ - see front matter
PII: S0142-727X(02)00186-8

Nomenclature

A_n, C_n, D_n, Y_n, and Φ_n	various coefficients of the solutions	V	radial velocity
Ca	capillary number	$\mathbf{v}$	velocity vector
g	gravity	V_o	velocity of outer moving wall
Gr	Grashof number $(g\alpha_1\Delta T R_2^3/\rho_1 v_1^2)$	z	axial direction
$\mathbf{n}$	unit normal outward	α	thermal expansion coefficient
p	pressure	β	ratio of length to outer radius (L/R_2)
Pr	Prandtl number (v/κ)	Γ	ratio of inner to outer radius (R_1/R_2)
r	radial direction	κ	thermal diffusivity
Re	Reynolds number (R_2V_o/v_1) or $(\sigma_1\Delta T R_2/\rho_1 v_1^2)$	μ	dynamic viscosity
R_1, R_2	distance to inner and outer radial wall	v	kinematic viscosity
$\mathbf{S}$	Cauchy stress tensor	ρ	density
t	time	σ_0	surface tension
$\mathbf{t}$	unit tangential vector	σ_1	change of surface tension with temperature
T	temperature	ω	vorticity
U	axial velocity	ψ	streamfunction
		ξ	interfacial deflection

caused in two different ways. The first is by moving the outer wall at a fixed velocity, which is a crude approximation of the effect that buoyancy-driven flow in the outer fluid has on the interface. The second way is by applying a vertical temperature gradient across the interface, causing Marangoni-driven flow. It will be shown that for Marangoni-driven flows, there exist certain viscosity ratios where the normal pressure and viscous stresses of the inner and outer fluid *nearly* cancel each other to create a flatter interface. Whereas for shear-driven flows, an increase in the outer viscosity only destabilizes the interface.

In Section 2, the model system will be described and an analytical solution to the fluid flow and interface shape is derived using an asymptotic expansion about a small capillary number. Section 3 presents a discussion on the results. Conclusions and future prospects of the work are given in the Section 4.

2. Mathematical model

In this section we will outline the assumptions made for the model liquid encapsulated liquid bridge. The model system is divided up into two different problems depending on whether we have shear-driven flow or Marangoni-driven flow (Fig. 1). For the shear-driven flow, there is no vertical temperature difference applied and an outer radial wall moving at a fixed velocity causes the fluid motion. For the Marangoni-driven flow, the outer radial wall is fixed and the fluid motion is generated by a vertical temperature difference that causes Marangoni stresses on the interface.

A viscous liquid encapsulated by another viscous liquid is suspended between two rigid rods. A rigid wall

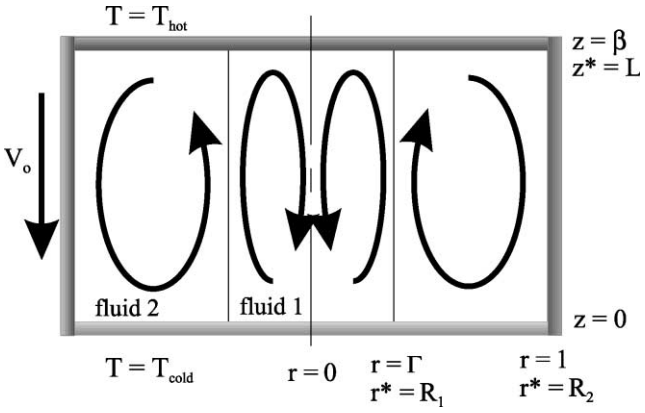

Fig. 1. Schematic diagram of the model. When the shear-driven flow is considered, the temperatures at the top and bottom wall are equal and constant, and the outer wall is moving with a constant velocity. When the Marangoni-driven flow is considered, a temperature difference is applied across the top and bottom wall, and the outer wall is fixed.

encloses the outer radius of the outer fluid. To simplify the analysis, we will assume that the fluid–fluid interface is initially flat and cylindrical. This assumption is valid for microgravity conditions or when the densities of the two fluids are identical. To further simplify the problem we will assume that both the shear-driven and the Marangoni-driven flows occur at very low Reynolds numbers. This will allow us to neglect the nonlinear terms, $\mathbf{v}\cdot\nabla\mathbf{v}$ and $\mathbf{v}\cdot\nabla T$ in the Navier–Stokes and energy equations, and decouples the temperature and velocity fields.

We start with the Boussinesq approximation to the axisymmetric continuity equation, momentum equation, and the energy equation in cylindrical coordinates.

$$\frac{\partial \widetilde{V}_i}{\partial \tilde{r}} + \frac{\widetilde{V}_i}{\tilde{r}} + \frac{\partial \widetilde{U}_i}{\partial \tilde{z}} = 0 \tag{1}$$

$$\rho_i\left[\frac{\partial \widetilde{V}_i}{\partial \tilde{t}}+\widetilde{V}_i\frac{\partial \widetilde{V}_i}{\partial \tilde{r}}+\widetilde{U}_i\frac{\partial \widetilde{V}_i}{\partial \tilde{z}}\right] = -\frac{\partial \tilde{p}_i}{\partial \tilde{r}}+\mu_i\left[\frac{\partial^2 \widetilde{V}_i}{\partial \tilde{r}^2}+\frac{1}{\tilde{r}}\frac{\partial \widetilde{V}_i}{\partial \tilde{r}}-\frac{\widetilde{V}_i}{\tilde{r}}+\frac{\partial^2 \widetilde{V}_i}{\partial \tilde{z}^2}\right] \quad (2)$$

$$\rho_i\left[\frac{\partial \widetilde{U}_i}{\partial \tilde{t}}+\widetilde{V}_i\frac{\partial \widetilde{U}_i}{\partial \tilde{r}}+\widetilde{U}_i\frac{\partial \widetilde{U}_i}{\partial \tilde{z}}\right] = -\frac{\partial \tilde{p}_i}{\partial \tilde{z}}+\mu_i\left[\frac{\partial^2 \widetilde{U}_i}{\partial \tilde{r}^2}+\frac{1}{\tilde{r}}\frac{\partial \widetilde{U}_i}{\partial \tilde{r}}+\frac{\partial^2 \widetilde{U}_i}{\partial \tilde{z}^2}\right]-g\rho(T) \quad (3)$$

$$\left[\frac{\partial \widetilde{T}_i}{\partial \tilde{t}}+\widetilde{V}_i\frac{\partial \widetilde{T}_i}{\partial \tilde{r}}+\widetilde{U}_i\frac{\partial \widetilde{T}_i}{\partial \tilde{z}}\right] = \kappa_i\left[\frac{\partial^2 \widetilde{T}_i}{\partial \tilde{r}^2}+\frac{1}{\tilde{r}}\frac{\partial \widetilde{T}_i}{\partial \tilde{r}}+\frac{\partial^2 \widetilde{T}_i}{\partial \tilde{z}^2}\right] \quad (4)$$

where $i=1$ is the inner fluid, $i=2$ is the outer fluid, V_i is the radial component of velocity, U_i is the axial component of velocity, p_i is the pressure, T_i is the temperature, ρ_i is the density, μ_i is the dynamic viscosity, v_i is the kinematic viscosity, κ_i is the thermal diffusivity, and g is gravity. The tildes ($\sim$) represent unscaled variables.

For the first analysis, we consider the shear-driven flow problem. Again, there is no applied temperature difference and we can therefore neglect the temperature in Eqs. (3) and (4). We will scale the length, velocity, time, and pressure by R_2, V_o, R_2/V_o, and R_2V_o/μ_1 respectively, where R_2 is the outer radius and V_o is the velocity of the outer moving wall. Under this scaling we introduce four dimensionless numbers.

$$\beta=\frac{L}{R_2},\quad \Gamma=\frac{R_1}{R_2},\quad \mu=\frac{\mu_2}{\mu_1},\quad \text{and}\quad Re=\frac{R_2V_o}{v_1} \quad (5)$$

Next, the radial and axial components of velocity are replaced by the Stokes's streamfunctions, ψ.

$$U_i=-\frac{1}{r}\frac{\partial \psi_i}{\partial r}\quad V_i=\frac{1}{r}\frac{\partial \psi_i}{\partial z} \quad (6)$$

After the curl of the momentum equation is taken, we arrive at the following fourth order system:

$$Re\frac{v_i}{v_1}\left[\frac{\partial \omega_i}{\partial t}+\frac{\partial}{\partial r}(V_i\omega_i)+\frac{\partial}{\partial z}(U_i\omega_i)\right]=\frac{1}{r}E^2\left(E^2\psi_i\right) \quad (7)$$

where $\omega_i=(\partial V_i)/(\partial z)-(\partial U_i)/(\partial r)$ is the vorticity and the operator E^2 is defined as:

$$E^2=\frac{\partial^2}{\partial r^2}-\frac{1}{r}\frac{\partial}{\partial r}+\frac{\partial^2}{\partial z^2} \quad (8)$$

As mentioned earlier, we will considerably simplify this problem by taking the zero Reynold's number limit, $Re\to 0$. The simplified domain equation to solve is:

$$E^2\left(E^2\psi_i\right)=0 \quad (9)$$

For the Marangoni-driven problem, the outer radial wall is fixed and a vertical temperature difference is applied. Here we will assume the density and surface tension are linear functions of the temperature.

$$\rho_i=\rho_i(T_c)+\left.\frac{\partial \rho_i}{\partial \widetilde{T}}\right|_{T_c}\left(\widetilde{T}_i-T_c\right)=\rho_{oi}-\alpha_i\left(\widetilde{T}_i-T_c\right)$$
$$\sigma=\sigma(T_c)+\left.\frac{\partial \sigma}{\partial \widetilde{T}}\right|_{T_c}\left(\widetilde{T}-T_c\right)=\sigma_0-\sigma_1\left(\widetilde{T}-T_c\right) \quad (10)$$

where σ is the surface tension of the liquid–liquid interface and the reference temperature, T_c, is the temperature at the bottom, cold rod.

For this problem, we need to use a different scaling. Here, we will scale the length, velocity, time, and pressure by R_2, $\sigma_1\Delta T/\mu_1$, $\mu_1R_2/\sigma_1\Delta T$, and $\sigma_1\Delta T/R_2$ respectively. After substituting the streamfunctions and taking the curl of the momentum equation we have:

$$Re\frac{\rho_i}{\rho_1}\left[\frac{\partial \omega_i}{\partial t}+\frac{\partial}{\partial r}(V_i\omega_i)+\frac{\partial}{\partial z}(U_i\omega_i)\right]=\frac{\mu_i}{\mu_1}\frac{1}{r}E^2\left(E^2\psi_i\right)+\frac{Gr}{Re}\frac{\alpha_i}{\alpha_1}\frac{\partial T_i}{\partial r} \quad (11)$$

$$RePr\frac{\kappa_1}{\kappa_i}\left[\frac{\partial T_i}{\partial t}+\frac{1}{r}\frac{\partial \psi_i}{\partial z}\frac{\partial T_i}{\partial r}-\frac{1}{r}\frac{\partial \psi_i}{\partial r}\frac{\partial T_i}{\partial z}\right]=\frac{\partial^2 T_i}{\partial r^2}+\frac{1}{r}\frac{\partial T_i}{\partial r}+\frac{\partial^2 T_i}{\partial z^2} \quad (12)$$

where $Pr=v_1/\kappa_1$, $Gr=(g\alpha_1\Delta TR_2^3)/(\rho_1v_1^2)$, and the Reynolds number is now defined as $Re=(\sigma_1\Delta TR_2)/(\rho_1v_1^2)$.

Again we take the small Reynolds number limit, while maintaining the ratio Gr/Re finite. The order of the Prandtl number is such that the product $PrRe$ is still small. When we solve for the steady temperature in Eq. (12), we find that the temperature is only a linear function of the axial direction.

$$T=\frac{\widetilde{T}-T_c}{\Delta T}=\frac{z}{\beta}$$

Therefore, the radial derivative of the temperature in the momentum equation is zero and the temperature and velocity fields decouple. Eqs. (11) and (12) will then simplify to Eq. (9). Notice that in the small Reynold's number limit, the domain equation for the Marangoni-driven problem is the same as the shear-driven problem. The difference between these two problems will of course be in the boundary conditions.

We now formulate the boundary conditions for the shear-driven and the Marangoni-driven problems. Again this problem will be simplified by employing a stress-free boundary condition at the top and bottom rods. The separation of variables technique can then be applied to the solution. Because the temperature field decouples from the velocity field for the Marangoni-driven problem, we will not show the boundary conditions for the temperature, except at the liquid–liquid

interface. It is necessary to account for the variation of the surface tension in the stress balance, but this will not change the linear temperature profile in the bulk of the fluid.

At the center of the inner fluid, we assume the velocity to be symmetric. At the top and bottom rods there is no penetration of fluids and a stress-free condition. There is also no fluid penetration at the interface and at the outer radial wall. For the shear-driven problem the axial velocity is equal to the velocity of the moving wall. For the Marangoni-driven problem, the outer wall is fixed with a no-slip condition.

The preceding assumptions lead to the following boundary conditions for the shear-driven problem:

$$\psi_i = 0, \quad \frac{\partial^2 \psi_i}{\partial z^2} = 0 \qquad \text{for } i = 1,2 \text{ and } z = 0, \beta \tag{13a}$$

$$\psi_1 = 0, \quad \frac{\partial^2 \psi_1}{\partial r^2} - \frac{1}{r}\frac{\partial \psi_1}{\partial r} = 0 \text{ at } r = 0 \tag{13b}$$

$$\psi_2 = 0 \quad \text{at } r = 1 \tag{13c}$$

$$\frac{\partial \psi_2}{\partial r} = 1 \quad \text{at } r = 1 \tag{13d}$$

and the following boundary conditions for the Marangoni-driven problem:

$$\psi_i = 0, \quad \frac{\partial^2 \psi_i}{\partial z^2} = 0 \qquad \text{for } i = 1,2 \text{ and } z = 0, \beta \tag{14a}$$

$$\psi_1 = 0, \quad \frac{\partial^2 \psi_1}{\partial r^2} - \frac{1}{r}\frac{\partial \psi_1}{\partial r} = 0 \text{ at } r = 0 \tag{14b}$$

$$\psi_2 = 0 \quad \text{at } r = 1 \tag{14c}$$

$$\frac{\partial \psi_2}{\partial r} = 0 \quad \text{at } r = 1 \tag{14d}$$

The remaining boundary conditions are determined by the stress balance and kinematic conditions at the interface:

The boundary conditions at the interface are governed by the following five equations.

$$\mathbf{n} \cdot \tilde{\mathbf{v}}_1 = \mathbf{n} \cdot \tilde{\mathbf{v}}_2 \tag{15a}$$

$$\mathbf{t} \cdot \tilde{\mathbf{v}}_1 = \mathbf{t} \cdot \tilde{\mathbf{v}}_2 \tag{15b}$$

$$\frac{\partial \tilde{\xi}}{\partial \tilde{t}} + \frac{\partial \tilde{\xi}}{\partial \tilde{z}} \widetilde{U}_1 = \widetilde{V}_1 \tag{15c}$$

$$\mathbf{t} \cdot \widetilde{\mathbf{S}}_1 \cdot \mathbf{n} - \mathbf{t} \cdot \widetilde{\mathbf{S}}_2 \cdot \mathbf{n} - \mathbf{t} \cdot \widetilde{\nabla}\sigma = 0 \tag{15d}$$

$$\mathbf{n} \cdot \widetilde{\mathbf{S}}_1 \cdot \mathbf{n} - \mathbf{n} \cdot \widetilde{\mathbf{S}}_2 \cdot \mathbf{n} + \sigma\left(\widetilde{\nabla} \cdot \mathbf{n}\right) = 0 \tag{15e}$$

where $\mathbf{S}_i$ is the Cauchy stress tensor, $\mathbf{n}$ and $\mathbf{t}$ are the unit normal and tangential vectors and ξ is the position of the interface.

$$\widetilde{\mathbf{S}}_i = -\tilde{p}_i \mathbf{I} + \mu_i \left[\widetilde{\nabla}\tilde{\mathbf{v}} + \left(\widetilde{\nabla}\tilde{\mathbf{v}}\right)^{\mathrm{T}}\right] \tag{16a}$$

$$\mathbf{n} = N^{-1}(1, -\xi_z)^{\mathrm{T}} \tag{16b}$$

$$\mathbf{t} = N^{-1}(\xi_z, 1)^{\mathrm{T}} \tag{16c}$$

$$N = \sqrt{1 + \xi_z} \tag{16d}$$

where $\xi_z = \partial\xi/\partial z$. Substituting Eqs. (16a)–(16d) into Eqs. (15a)–(15e) gives:

$$\widetilde{U}_1 = \widetilde{U}_2 \tag{17a}$$

$$\widetilde{V}_1 = \widetilde{V}_2 \tag{17b}$$

$$\frac{\partial \tilde{\xi}}{\partial \tilde{z}} \widetilde{U}_1 = \widetilde{V}_1 \tag{17c}$$

$$\begin{aligned} &-\tilde{p}_1 + \frac{2\mu_1}{N^2}\left[\frac{\partial \widetilde{V}_1}{\partial \tilde{r}} - \tilde{\xi}_{\tilde{z}}\left(\frac{\partial \widetilde{U}_1}{\partial \tilde{r}} + \frac{\partial \widetilde{V}_1}{\partial \tilde{z}}\right) + \tilde{\xi}_{\tilde{z}}^2 \frac{\partial \widetilde{U}_1}{\partial \tilde{z}}\right] \\ &-\tilde{p}_2 + \frac{2\mu_2}{N^2}\left[\frac{\partial \widetilde{V}_2}{\partial \tilde{r}} - \tilde{\xi}_{\tilde{z}}\left(\frac{\partial \widetilde{U}_2}{\partial \tilde{r}} + \frac{\partial \widetilde{V}_2}{\partial \tilde{z}}\right) + \tilde{\xi}_{\tilde{z}}^2 \frac{\partial \widetilde{U}_2}{\partial \tilde{z}}\right] \\ &+ \sigma N^{-1}\left[\tilde{\xi}^{-1} - \frac{\tilde{\xi}_{\tilde{z}\tilde{z}}}{N^2}\right] = 0 \end{aligned} \tag{17d}$$

$$\begin{aligned} &\mu_1\left[\left(1 - \tilde{\xi}_{\tilde{z}}^2\right)\left(\frac{\partial \widetilde{U}_1}{\partial \tilde{r}} + \frac{\partial \widetilde{V}_1}{\partial \tilde{z}}\right) + 2\tilde{\xi}_{\tilde{z}}\left(\frac{\partial \widetilde{V}_1}{\partial \tilde{r}} - \frac{\partial \widetilde{U}_1}{\partial \tilde{z}}\right)\right] \\ &+ \mu_2\left[\left(1 - \tilde{\xi}_{\tilde{z}}^2\right)\left(\frac{\partial \widetilde{U}_1}{\partial \tilde{r}} + \frac{\partial \widetilde{V}_1}{\partial \tilde{z}}\right) + 2\tilde{\xi}_{\tilde{z}}\left(\frac{\partial \widetilde{V}_1}{\partial \tilde{r}} - \frac{\partial \widetilde{U}_1}{\partial \tilde{z}}\right)\right] \\ &- \frac{\Delta T \sigma_1}{\beta} = 0 \end{aligned} \tag{17e}$$

We next substitute in the appropiate scaling and streamfunctions to get the following equations for the shear-driven problem.

$$\psi_1 = \psi_2 \quad \text{at } r = \Gamma \tag{18a}$$

$$\frac{\partial \psi_1}{\partial r} = \frac{\partial \psi_2}{\partial r} \quad \text{at } r = \Gamma \tag{18b}$$

$$\xi_z \frac{\partial \psi_1}{\partial z} = \frac{\partial \psi_2}{\partial z} \quad \text{at } r = \Gamma \tag{18c}$$

$$\begin{aligned} &2Ca\left\{\left(1 - \xi_z^2\right)\frac{1}{r}\frac{\partial^2 \psi_1}{\partial r \partial z} - \frac{1}{r^2}\frac{\partial \psi_1}{\partial z} - \xi_z\left[\frac{1}{r}\left(\frac{\partial^2 \psi_1}{\partial z^2} - \frac{\partial^2 \psi_1}{\partial r^2}\right)\right.\right. \\ &\left.\left. + \frac{1}{r^2}\frac{\partial \psi_1}{\partial r}\right]\right\} - 2\mu Ca\left\{\left(1 - \xi_z^2\right)\frac{1}{r}\frac{\partial^2 \psi_2}{\partial r \partial z} - \frac{1}{r^2}\frac{\partial \psi_2}{\partial z}\right. \\ &\left. - \xi_z\left[\frac{1}{r}\left(\frac{\partial^2 \psi_2}{\partial z^2} - \frac{\partial^2 \psi_2}{\partial r^2}\right) + \frac{1}{r^2}\frac{\partial \psi_2}{\partial r}\right]\right\} \\ &+ CaN^2(P_2 - P_1) + N\left[\xi^{-1} - \frac{\xi_{zz}}{N^2}\right] = 0 \end{aligned} \tag{18d}$$

$$\left\{(1-\xi_z^2)\left[\frac{1}{r}\left(\frac{\partial^2\psi_1}{\partial z^2}-\frac{\partial^2\psi_1}{\partial r^2}\right)+\frac{1}{r^2}\frac{\partial\psi_1}{\partial r}\right]-\frac{2}{r^2}\xi_z\left(\frac{\partial\psi_1}{\partial z}\right)\right\} - \mu\left\{(1-\xi_z^2)\left[\frac{1}{r}\left(\frac{\partial^2\psi_2}{\partial z^2}-\frac{\partial^2\psi_2}{\partial r^2}\right)+\frac{1}{r^2}\frac{\partial\psi_2}{\partial r}\right] - \frac{2}{r^2}\xi_z\left(\frac{\partial\psi_2}{\partial z}\right)\right\}=0 \tag{18e}$$

where Ca is the Capillary number, which is defined differently for the shear-driven and the Marangoni-driven problem.

$$Ca=\frac{\mu V_o}{\sigma_0} \text{ or } \frac{\sigma_1\Delta T}{\sigma_0}$$

For the Marangoni-driven problem, the only equation which is different is Eq. (18e).

$$\left\{(1-\xi_z^2)\left[\frac{1}{r}\left(\frac{\partial^2\psi_1}{\partial z^2}-\frac{\partial^2\psi_1}{\partial r^2}\right)+\frac{1}{r^2}\frac{\partial\psi_1}{\partial r}\right]-\frac{2}{r^2}\xi_z\left(\frac{\partial\psi_1}{\partial z}\right)\right\} - \mu\left\{(1-\xi_z^2)\left[\frac{1}{r}\left(\frac{\partial^2\psi_2}{\partial z^2}-\frac{\partial^2\psi_2}{\partial r^2}\right)+\frac{1}{r^2}\frac{\partial\psi_2}{\partial r}\right] - \frac{2}{r^2}\xi_z\left(\frac{\partial\psi_2}{\partial z}\right)\right\}+\frac{\Gamma}{\beta}=0 \tag{19}$$

Closely following the paper by Kuhlman (1989), the dependent variables ψ_i, P_i, and ξ will be expanded in terms of the Capillary number.

$$\psi_i=\sum_{\substack{m=0\\n=1\\p=0}}^{\infty} Ca^m Re^n Pr^p \psi_{im}(r,z) \tag{20}$$

$$P_i=\frac{Re}{Ca}P_{is}+\sum_{\substack{m=0\\n=1\\p=0}}^{\infty} Ca^m Re^n Pr^p P_{im}(r,z) \tag{21}$$

$$\xi=\xi_s(z)+\sum_{\substack{m=1\\n=0\\p=0}}^{\infty} Ca^m Re^n Pr^p \xi_m(r,z) \tag{22}$$

The first term of the pressure expansion is justified on physical grounds by setting the velocity equal to zero in Eq. (18d). The surface deflection will be balanced by the pressure only if the pressure is proportional to the inverse of the Capillary number. The two terms in Eq. (18d), ξ^{-1} and N, can be expanded in a Taylor series assuming that $Ca\xi_1/\Gamma \ll 1$ and $Ca\,\partial\xi_1/\partial z \ll 1$, so that $\xi^{-1} \cong (\Gamma - Ca\xi_1)/\Gamma^2 + \mathrm{O}(Ca^2)$ and $N \cong 1 + \mathrm{O}(Ca^2)$. As was stated earlier, we will assume that the interface shape is cylindrical for the zeroth order Capillary term, $\xi_s(z)=\Gamma$. The terms in Eqs. (20)–(22) are expanded to the lowest order $\mathrm{O}(Re^1, Pr^0, Ca^0)$. To simplify the notation, the subscripts n and p will be dropped and only the subscript for the Capillary term, m, will be kept.

After substituting Eqs. (20)–(22) into Eqs. (18a)–(18e) and (19), the zeroth order capillary number boundary conditions at the interface for the shear-driven problem become:

$$\psi_{10}=\psi_{20}=0 \quad \text{at } r=\Gamma \tag{23a}$$

$$\frac{\partial\psi_{10}}{\partial r}=\frac{\partial\psi_{20}}{\partial r} \quad \text{at } r=\Gamma \tag{23b}$$

$$\frac{\partial^2\psi_{10}}{\partial r^2}-\frac{1}{\Gamma}\frac{\partial\psi_{10}}{\partial r}=\frac{\partial^2\psi_{20}}{\partial r^2}-\frac{1}{\Gamma}\frac{\partial\psi_{20}}{\partial r} \quad \text{at } r=\Gamma \tag{23c}$$

The zeroth-order Capillary boundary conditions at the interface for the Marangoni-driven problem are:

$$\psi_{10}=\psi_{20}=0 \quad \text{at } r=\Gamma \tag{24a}$$

$$\frac{\partial\psi_{10}}{\partial r}=\frac{\partial\psi_{20}}{\partial r} \quad \text{at } r=\Gamma \tag{24b}$$

$$\frac{\partial^2\psi_{10}}{\partial r^2}-\frac{1}{\Gamma}\frac{\partial\psi_{10}}{\partial r}-\frac{\partial^2\psi_{20}}{\partial r^2}-\frac{1}{\Gamma}\frac{\partial\psi_{20}}{\partial r}-\frac{\Gamma}{\beta} \quad \text{at } r=\Gamma \tag{24c}$$

We may now compare the boundary conditions for the shear-driven and Marangoni-driven problems. It was already noted that the domain equations for both problems are the same (Eq. (9)). Therefore, the two problems only differ by two boundary conditions, Eqs. (13d) and (14d), and Eqs. (23c) and (24c). This observation will be very helpful in solving the two problems.

The form of the solution can be found in a related problem given by Duda and Vrentas (1971a,b). By applying boundary conditions (13a)–(13c) and (23a) for the shear-driven and Marangoni-driven problem, we arrive at the following form of the solution:

$$\psi_{10}=\sum_{n=1}^{\infty} A_n F_n(r)\sin(a_n z) \tag{25}$$

$$\psi_{20}=\sum_{n=1}^{\infty}\left[C_n G_n(r)+D_n H_n(r)\right]\sin(a_n z) \tag{26}$$

where A_n, C_n, and D_n are constants and F_n, G_n, and H_n are defined below.

$$F_n(r)=\frac{\Gamma r I_1(a_n r)I_2(a_n\Gamma)-r^2 I_1(a_n\Gamma)I_2(a_n r)}{I_2^2(a_n\Gamma)} \tag{27}$$

$$G_n(r)=r^2 I_2(a_n r)+B_{2n} r I_1(a_n r)+B_{3n} r K_1(a_n r) \tag{28}$$

$$H_n(r)=r^2 K_2(a_n r)+B_{4n} r I_1(a_n r)+B_{5n} r K_1(a_n r) \tag{29}$$

Here I_m and K_m represent the mth order modified Bessels function of the first and second kind, respectively, where $a_n = n\pi/\beta$, and the constants B_{in} are defined as:

$$
\begin{aligned}
B_{1n} &= K_1(a_n\Gamma)I_1(a_n) - K_1(a_n)I_1(a_n\Gamma)\\
B_{2n} &= \frac{\Gamma I_2(a_n\Gamma)K_1(a_n) - K_1(a_n\Gamma)I_2(a_n)}{B_{1n}}\\
B_{3n} &= \frac{I_1(a_n\Gamma)I_2(a_n) - \Gamma I_1(a_n)I_2(a_n\Gamma)}{B_{1n}}\\
B_{4n} &= \frac{\Gamma K_2(a_n\Gamma)K_1(a_n) - K_2(a_n)K_1(a_n\Gamma)}{B_{1n}}\\
B_{5n} &= \frac{K_2(a_n)I_1(a_n\Gamma) - \Gamma K_2(a_n\Gamma)I_1(a_n)}{B_{1n}}
\end{aligned}
\tag{30}
$$

Because the boundary conditions that have been applied, are the same for both the shear-driven and Marangoni-driven problems, Eqs. (25)–(30) hold for both problems. All that remains now, is to solve for the remaining three constants A_n, C_n, and D_n. These three constants, however, will be different for the shear-driven and Marangoni-driven problems.

We start with the shear-driven problem and apply its remaining three boundary conditions (13d), (23b), and (23c).

$$C_nG_n'(1) + D_nH_n'(1) = b_n \tag{31}$$

$$A_nF_n'(\Gamma) = C_nG_n'(\Gamma) + D_nH_n'(\Gamma) \tag{32}$$

$$
\begin{aligned}
&A_n\left[F_n''(\Gamma) - \frac{1}{\Gamma}F_n'(\Gamma)\right]\\
&\quad = \mu\left\{C_n\left[G_n''(\Gamma) - \frac{1}{\Gamma}G_n'(\Gamma)\right] + D_n\left[H_n''(\Gamma) - \frac{1}{\Gamma}H_n'(\Gamma)\right]\right\}
\end{aligned}
\tag{33}
$$

where the prime denotes differentiation with respect to r, and b_n are the odd Fourier coefficients defined as:

$$\sum_{n=1}^{\infty} b_n \sin(a_nz) = 1 \tag{34}$$

Eq. (33) can be substantially simplified by the following formulas:

$$\left[F_n''(\Gamma) - \frac{1}{\Gamma}F_n'(\Gamma)\right] = -2a_n\Gamma\frac{I_1^2(a_n\Gamma)}{I_2^2(a_n\Gamma)} \tag{35a}$$

$$\left[G_n''(\Gamma) - \frac{1}{\Gamma}G_n'(\Gamma)\right] = 2a_n\Gamma I_1(a_n\Gamma) \tag{35b}$$

$$\left[H_n''(\Gamma) - \frac{1}{\Gamma}H_n'(\Gamma)\right] = -2a_n\Gamma K_1(a_n\Gamma) \tag{35c}$$

Substituting Eq. (35a)–(35c) into Eq. (33) and simplifying gives:

$$A_n = \frac{b_n}{F_n'(\Gamma)}\frac{G_n'(\Gamma)\Phi_n + H_n'(\Gamma)}{G_n'(1)\Phi_n + H_n'(1)} \tag{36}$$

$$C_n = \frac{b_n\Phi_n}{G_n'(1)\Phi_n + H_n'(1)} \tag{37}$$

$$D_n = \frac{b_n}{G_n'(1)\Phi_n + H_n'(1)} \tag{38}$$

where Φ_n is defined as

$$\Phi_n = \frac{\mu K_1(a_n\Gamma)F_n'(\Gamma) - H_n'(\Gamma)(I_1^2(a_n\Gamma)/I_2^2(a_n\Gamma))}{\mu I_1(a_n\Gamma)F_n'(\Gamma) + G_n'(\Gamma)(I_1^2(a_n\Gamma)/I_2^2(a_n\Gamma))} \tag{39}$$

For the Marangoni-driven problem, we apply the three boundary conditions (24b), (24c), and (14d) to Eqs. (25) and (26). The solution for the three coefficients A_n, C_n, and D_n become:

$$A_n = \frac{H_n'(1)G_n'(\Gamma) - H_n'(\Gamma)G_n'(1)}{H_n'(1)F_n'(\Gamma)}D_n = Q_nD_n \tag{40}$$

$$C_n = -\frac{H_n'(1)}{G_n'(1)}D_n \tag{41}$$

$$D_n = \frac{b_n}{2a_n\Gamma\beta M_n} \tag{42}$$

$$M_n = \frac{\mu}{U_n'(1)}\left[G_n'(1)I_1(a_n\Gamma) + H_n'(1)K_1(a_n\Gamma)\right] - Q_n\frac{I_1^2(a_n\Gamma)}{I_2^2(a_n\Gamma)} \tag{43}$$

The final equation we need to solve is the first-order Capillary number correction to the surface deflection. To do this, substitute Eqs. (20)–(22) in the normal stress balance, Eq. (18d), and take the $O(Ca)$ terms.

$$\frac{d^2\xi_1}{dz^2} + \frac{1}{\Gamma^2}\xi_1 = \left[\frac{2}{\Gamma}\left(\frac{\partial^2\psi_{10}}{\partial r\partial z} - \mu\frac{\partial^2\psi_{20}}{\partial r\partial z}\right) + P_{20} - P_{10}\right]_{r=\Gamma} \tag{44}$$

We can think of Eq. (44) as a second-order ordinary differential equation with a relatively complicated forcing function. The first two terms in the forcing function represents the shear stress applied to the inner and outer fluid, respectively. The last two terms represent the dynamic pressure acting on the interface.

Notice that quite conveniently, the first order correction to the surface deflection depends only on the zeroth-order streamfunctions and pressures. The pressure in Eq. (44) may be found from Eq. (2), after the appropiate scaling.

$$\frac{\partial P_{10}}{\partial r} = \frac{1}{r}\frac{\partial}{\partial z}\left(E^2\psi_{10}\right) \tag{45}$$

$$\frac{\partial P_{20}}{\partial r} = \frac{\mu}{r}\frac{\partial}{\partial z}\left(E^2\psi_{20}\right) \tag{46}$$

Substitution of Eqs. (25), (26), (45) and (46) into Eq. (44) yields:

$$\frac{d^2\xi_1}{dz^2} + \frac{1}{\Gamma^2}\xi_1 = \sum_{n=1}^{\infty} Y_n\cos(a_nz) \tag{47}$$

$$Y_n = 2a_n\left\{A_n\left[\frac{F_n'(\Gamma)}{\Gamma}+\frac{I_0(a_n\Gamma)I_1(a_n\Gamma)}{I_2^2(a_n\Gamma)}\right]+\mu C_n\left[I_0(a_n\Gamma)-\frac{G_n'(\Gamma)}{\Gamma}\right]+\mu D_n\left[K_0(a_n\Gamma)-\frac{H_n'(\Gamma)}{\Gamma}\right]\right\}$$

The solution of (47) is given as:

$$\xi_1(z)=\sum_{n=1}^{\infty}\frac{Y_n\beta^2}{n^2\pi^2-(\beta/\Gamma)^2}\left\{\cos(z/\Gamma)-\cos\left(\frac{n\pi z}{\beta}\right)+\frac{\sin(z/\Gamma)}{\sin(\beta/\Gamma)}[(-1)^n-\cos(\beta/\Gamma)]\right\} \tag{48}$$

By evaluating the proper limiting form of (48), it can be shown that a singularity exist at $\beta/\Gamma = 2\pi$. As $\beta/\Gamma \to 2\pi$, the surface deflection becomes large and the assumption that $Ca\xi_1/\Gamma \ll 1$ becomes invalid. Therefore, (48) only holds for $0 < \beta/\Gamma < 2\pi$.

In this section, we analytically derived the equations for the streamfunctions and the surface deflection for both the shear-driven and Marangoni-driven problems. The form of the solutions for both problems are the same and only differ by the constants, A_n, C_n, and D_n for the streamfunctions, and Y_n for the surface deflections. In the next section, we will look at the functional dependence of the solutions on the viscosity ratio μ, and the two geometric parameters β and Γ.

3. Results and discussion

In this section, we will determine the behavior of the shear function and the surface deflections as a function of the geometric parameters β and Γ, as well as the viscosity ratio, μ. This will be done for both the shear-driven and the Marangoni-driven problems.

3.1. Shear-driven flow

We start by noting that $I_m(r)$ and $K_m(r)$ are positive and real for m an integer and r real. Next we analyze the coefficients of the stream function: A_n, C_n, D_n, and Φ_n. By calculating all possible values of β and Γ for $G_n'(\Gamma)$, $H_n'(\Gamma)$, $G_n'(1)$, $H_n'(1)$, and $F_n'(\Gamma)$ (i.e. $0 < \beta < 2\pi$, and $0 < \Gamma < 1$), it can be shown that $G_n'(\Gamma) < 0$, $H_n'(\Gamma) > 0$, $G_n'(1) > 0$, $H_n'(1) < 0$, and $F_n'(\Gamma) < 0$. Using this, we can write the functional form of Φ_n as:

$$\Phi_n = -\frac{a\mu+b}{c\mu+d} \tag{49}$$

where a, b, c, and $d > 0$ are constants with respect to μ, and

$$\frac{\partial\Phi_n}{\partial\mu} = -\frac{bc-ad}{(c\mu+d)^2} \tag{50}$$

To determine whether Φ_n contains a minimum or maximum, we calculate the values of a, b, c, and d and show that $ad - bc > 0$ for all values of β and Γ, therefore $\partial\Phi_n/\partial\mu > 0$. From these results it follows that

$$\frac{\partial A_n}{\partial\mu} > 0,\ \frac{\partial C_n}{\partial\mu} < 0,\ \frac{\partial D_n}{\partial\mu} < 0 \quad \text{and } A_n, C_n, D_n, Y_n > 0 \tag{51}$$

Therefore as the viscosity ratio increases, the velocity of the outer fluid decreases, while the velocity of the inner fluid increases. For example, if the outer viscosity increases relative to the inner viscosity, the outer fluid slows down and the inner fluid speeds up. This can be explained by noting that the outer wall in the shear-driven flow is held constant, so that the velocity in the outer fluid will remain relatively constant as the viscosity ratio increases. The velocity of the inner fluid, though, will increase as the higher viscosity of the outer fluid increases the shear rate on the interface.

Plots of the streamfunction for various values of β and Γ for a fixed $\mu = 10$ are given in Fig. 2. Here two qualitative trends can be seen. As $\beta = L/R_2$ increases, the flow in both the inner and outer fluid increases, although the largest velocity occurs in the outer fluid. When $\Gamma = R_1/R_2$ increases, the flow in the outer fluid decreases and the flow in the inner fluid increases. The reason being that as the interface moves closer to the outer moving wall, more of the momentum is transferred to the inner fluid.

To analyze the surface deflection dependence on the viscosity ratio, we will again find how the coefficient $Y_n(\beta,\Gamma,\mu)$ depends on the viscosity ratio. Here the values of $\partial Y_n/\partial\mu$ are calculated numerically, which shows that $\partial Y_n/\partial\mu > 0$ for all reasonable values of μ, β, and Γ. Therefore the surface deflections in the shear-driven problem increase monotonically with an increase in the viscosity ratio and do not have a minimum value with respect to changes in the viscosity ratio. This can be explained physically by looking at Eq. (44). The first term on the right-hand side of Eq. (44) represents the shear from the inner fluid, the second term represents the shear from the outer fluid, and the third and fourth term represents the dynamic pressure of the outer and inner fluid, respectively. In the shear-driven flow, all of the shear in the inner fluid is generated by shearing of the outer fluid. Apparently because of this, no matter what the value of μ is, the shearing in the inner fluid never equals that of the outer fluid. As the viscosity increases, the shear force in the outer fluid increases faster than the shear force in the inner fluid. This, as we will see in the next section, is not true for the Marangoni-driven flow. However, there are several terms in $\partial Y_n/\partial\mu$ that are negative, which gives at least the theoretical possibility that the surface may have a minimum, but apparently does not for this derivation.

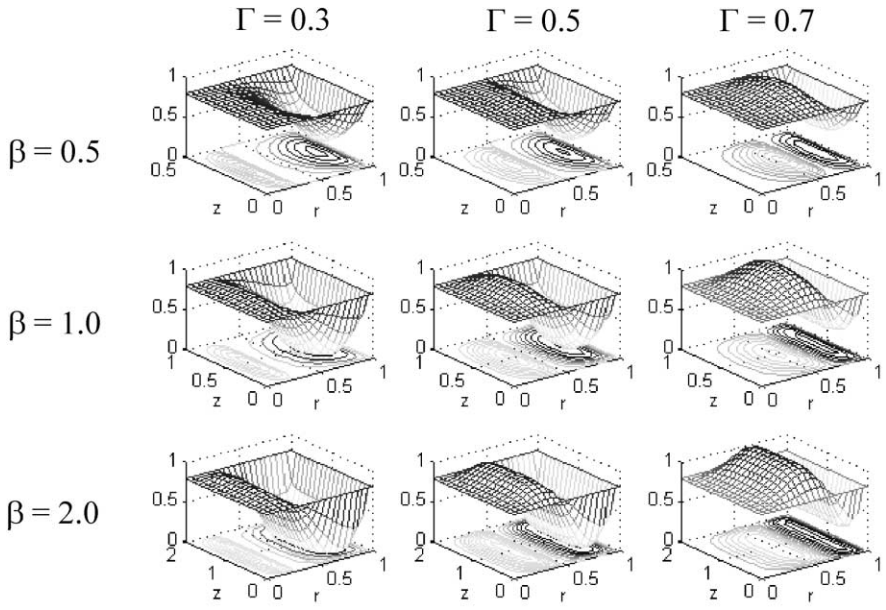

Fig. 2. Streamfunction plots for the shear-driven flow for various Γ and β ($\mu = 10$).

3.2. Marangoni-driven flow

In this section we will perform a similar analysis to that of the previous section. This will be done by analyzing the coefficients A_n, C_n, and D_n for the stream functions, and the coefficient Y_n for the surface deflections. As a reminder, the outer radial wall is no longer moving and the flow is generated solely by the thermocapillary movement of the fluid–fluid interface.

We begin this section with the same analysis as in the shear-driven flow. The coefficients of the stream function A_n, C_n, and D_n are evaluated for all values of β and Γ for a fixed μ (Fig. 3). Here we find that the behavior of the streamfunctions to be quite different than the shear-driven flow. The streamfuncions, in general, decrease as β increases. For small values of $\beta = L/R_2$ as $\Gamma = R_1/R_2$ increases the inner and outer streamfunctions increase. The streamfunction of the outer fluid seems to reach a maximum around $\Gamma = 0.5$, where the width of the inner and outer fluid are equal. As Γ increases further, the velocity in the outer fluid decreases. This makes sense when we consider that as the interface moves closer to the stationary outer wall, there is less room for the outer fluid to move and therefore slows down. The inner

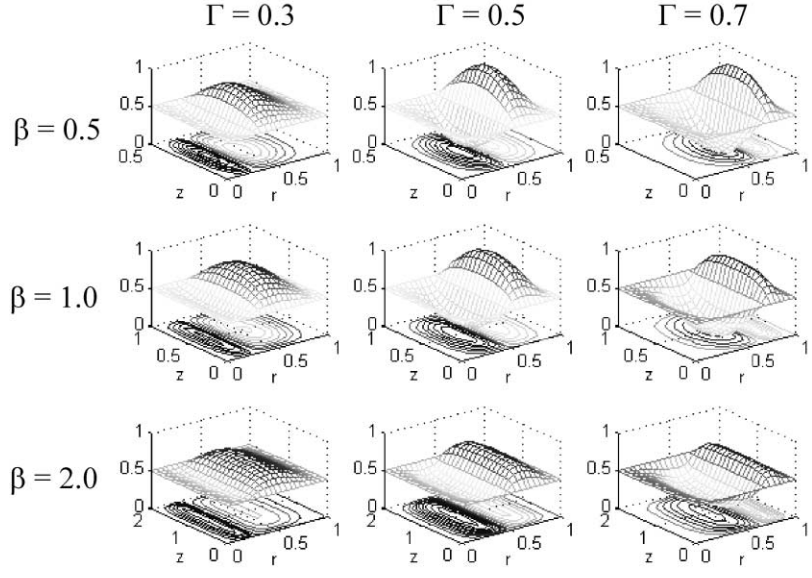

Fig. 3. Streamfunction plots for the Marangoni-driven flow for various Γ and β ($\mu = 1$).

fluid on the other hand seems to increase further as $\Gamma \to 1$.

Evaluating the behavior of the coefficients of the streamfunction as a function of the viscosity ratio also exhibit different behavior. Here we find that

$$\frac{\partial A_n}{\partial \mu} > 0, \quad \frac{\partial C_n}{\partial \mu} < 0, \quad \frac{\partial D_n}{\partial \mu} < 0$$
$$\text{and that } A_n < 0, \ C_n > 0, \text{ and } D_n > 0 \tag{52}$$

Therefore as the viscosity ratio increases, both the inner and outer velocities decrease. In one instance, this makes sense. As the outer viscosity increases, the viscosity ratio increases and both fluids will slow down because the outer fluid's thicker consistency makes it more difficult to move the two fluids. In the opposite scenario, though, this argument does not agree. As the inner viscosity increases, the viscosity ratio decreases, and we find that both fluid velocities increase. It could be weakly argued that the larger inner viscosity creates a larger shear force on the outer fluid and therefore increases the outer fluids velocity. Apparently the different boundary conditions that the two fluids experience plays a significant role in the fluid flow.

The most interesting result of this study comes from analyzing the behavior of the interface as a function of the viscosity ratio. Here we find that for a fixed value of β, Γ, and n, the coefficient Y_n is negative for small values of μ and positive for larger values of μ. This indicates that at a particular value of μ, the interface goes to zero. However, this is only true for the one fixed value of n (say $n = 1$). For a different value of n (say $n = 3$), the coefficient Y_n is zero at a different value of μ. The net result is that the interface becomes nearly zero for a particuar value of μ (Fig. 4).

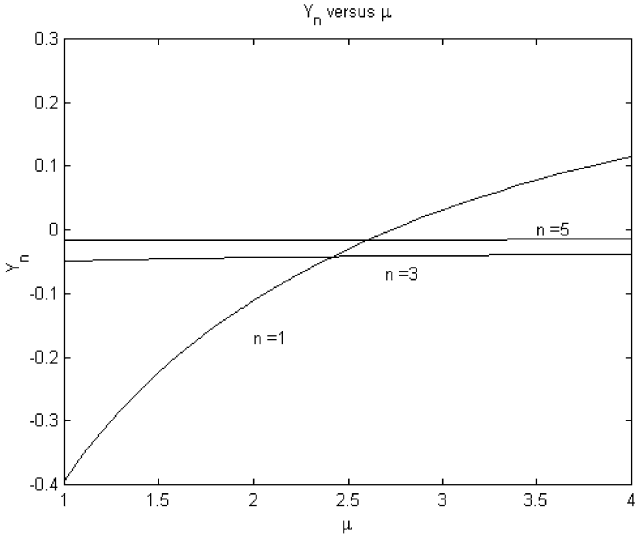

Fig. 4. Plot of the surface deflection coefficient Y_n versus the viscosity ratio for values of $n = 1$, 3, and 5. Note that the values of the coefficient for different n do not cross the axis at the same location.

Fig. 5a gives a plot of the axial direction, z, versus the interface deflection, ξ. From the plot we see that for the values of $\mu > 2.75$, the upper interface deflects outward, and that for the values of $\mu < 2.25$ the upper interface deflects inward. The change in direction of deflection is caused by the change in the viscous stress acting on the interface.

Fig. 5b shows the interface deflections for values of $\mu = 2.4$, 2.5, and 2.6. Here we can see that the interface also changes the direction of deflection, but now the interface appears to have more harmonics or modes associated with it. This can be explained, as stated above, in terms of the different values of n. For example, say that the value of the viscosity is such that the first coefficient of the interface deflection, Y_1, is exactly zero. However, the other coefficients (Y_n for $n > 2$) will not be zero for the same value of μ. As each n is associated with the harmonic term $\sin(a_n z)$, the first harmonic of the interface will be cancelled out, but not the higher harmonics. Therefore the total interface deflection will not be zero, but will be considerably smaller (compare the values of the interface deflections between Fig. 5a and b), because each consecutive value of Y_n will be smaller than the preceeding value (as it must for a converging series). We can conclude that the interface can never be made exactly flat by adjusting the viscosity ratio alone.

4. Conclusions

In this paper, an analytical derivation of the surface deflections was given assuming that the interface in the absence of flow, was perfectly cylindrical and flat. The surface deflection was found up to the first order in the Capillary number, Ca. Using these derivations, the streamfunctions and the surface deflections were analyzed by varying the two geometric parameters, β and Γ, and the viscosity ratio, μ. Two distinctly different cases were investigated. In the first case, the flow was generated by a moving outer wall (the shear-driven flow), and in the second case, the flow was generated by the Marangoni stress caused by a temperature difference across the top and bottom walls (the Marangoni-driven flow).

For the shear-driven flow, as the viscosity ratio increased, the velocity in the inner fluid increased, while the velocity of the outer fluid decreased. For the Marangoni-driven flow, as the viscosity ratio increased, the velocities in both fluids decreased. In both flow situations, the velocities were seen to be a reasonably strong function of the geometric parameters, β and Γ.

The main result of this paper elucidated the behavior of the interfacial deflection as the viscosity ratio of the two fluids were varied. It was found that for the shear-driven flow, as the viscosity ratio increased, the surface deflections increased. This was explained by the fact that the flow in the inner fluid was only generated by the

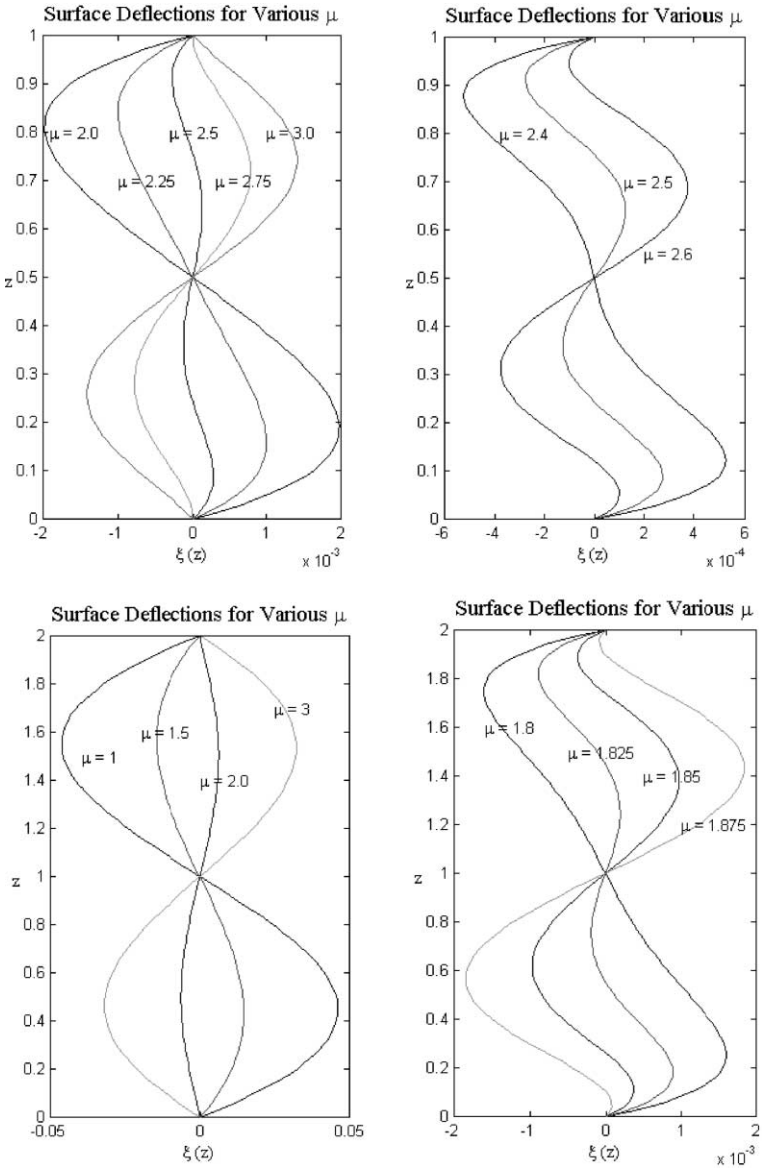

Fig. 5. Plot of the liquid height versus the surface deflection for various values of the viscosity ratio, μ. In (a) and (b) $\Gamma = 0.5$, $\beta = 1$ and in (c) and (d) $\Gamma = 0.5$, $\beta = 2$. When the surface deflections become small, higher modes ($n > 3$) are seen.

shearing of the outer fluid. Therefore, the shear forces from the two fluids were never able to balance each other out. The shear exerted by the outer fluid always exceeded the shear exerted by the inner fluid.

For the Marangoni-driven flow, it was possible to find values of the viscosity ratio where the shear forces nearly canceled each other out. More precisely, each harmonic or mode of the surface deflection had a particular value of the viscosity ratio where that mode would become identically zero. However, these values of the viscosity ratio were not the same for each mode, and therefore the interface never became exactly flat. It would be very interesting to see if this were true in an actual experiment (Lowry and Steen, 1995). For example, if one desired to adjust the viscosity ratio in a liquid encapsulated liquid bridge in order to minimize the interfacial deflections, it would be logical to find two fluids whose viscosity ratio exactly cancelled out the first (and largest) mode. However, as the temperature difference increased, the second and higher modes ($n = 3, 5, 7, \ldots$) would begin to grow.

Obvious extensions to this problem would be to include more realistic no-slip boundary conditions on the top and bottom walls, and an initially deformed interface to account for fluids where the densities are not identically equal. The no-slip condition would involve the semi-analytical Papokovich–Fadle functions (Joseph, 1977), but the deformed interface would require a more involved numerical computation. It would also be interesting to account for the variation of the viscosity

as a function of temperature, where the change in viscosity would create differences in the shear stress on the interface.

Acknowledgements

The author would like to thank the NSF-NATO postdoctoral fellowship, grant number DGE-9710743 for funding and support. The author would also like to thank Dr. J.C. Legros and the other members of the Microgravity Research Center at the Université Libre de Bruxelles for their hospitality.

References

Duda, J.L., Vrentas, J.S., 1971a. Steady flow in the region of closed streamlines in a cylindrical cavity. J. Fluid Mech. 45, 247–260.

Duda, J.L., Vrentas, J.S., 1971b. Heat transfer in a cylindrical cavity. J. Fluid Mech. 45, 261–279.

Hurle, D.T.J., 1994. Handbook of crystal growth. North-Holland, Amsterdam.

Joseph, D.D., 1977. The convergence of biorthogonal series for biharmonic and stokes flow egde problems: part 1. SIAM J. Appl. Math. 33, 337–347.

Kuhlman, H., 1989. Small amplitude thermocapillary flow and surface deformations in a liquid bridge. Phys. Fluids A 1, 672–677.

Lowry, B.J., Steen, P.H., 1995. Stability of slender liquid bridges subjected to axial flows. J. Fluid Mech. 330, 189–213.

Rybicki, A., Floryan, J.M., 1983a. Thermocapillary effects in liquid bridges. I. Thermocapillary convection. Phys. Fluids 30 (7), 1956–1972.

Rybicki, A., Floryan, J.M., 1983b. Thermocapillary effects in liquid bridges. II. Deformation of the interface and capillary instability. Phys. Fluids 30 (7), 1973–1983.

Wanschura, M., Shevtsova, V.M., Kuhlmann, H.C., Rath, H.J., 1995. Convective instability mechanisms in thermocapillary liquid bridges. Phys. Fluids 7 (5), 912–925.